Revealing microstructural degradation mechanism induced by interdiffusion between Amdry365 coating and IN792 superalloy

Materials & Design 241 (2024) 112937

Contents lists available at ScienceDirect

Materials & Design

journal homepage: www.elsevier.com/locate/matdes

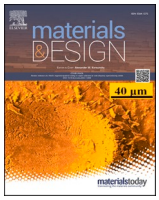

Revealing microstructural degradation mechanism induced by interdiffusion between Amdry365 coating and IN792 superalloy

Xiaoyu Sun [a], Xiaolong Li [b], Sheng Guo [b], Xin Yu [c], Lilong Zhu [c], Jianwei Teng [c], Liang Jiang [c], Johan Moverare [a], Xin-Hai Li [d], Ru Lin Peng [a,*]

[a] Department of Management and Engineering, Linköping University, SE-58183 Linköping, Sweden
[b] Department of Industrial and Materials Science, Chalmers University of Technology, Gothenburg SE-41296, Sweden
[c] Institute for Advanced Studies in Precision Materials, Yantai University, Yantai, Shandong 264005, China
[d] Siemens Energy AB, SE-61283 Finspång, Sweden

ARTICLE INFO

Keywords:
Bond coating
Interdiffusion
Microstructural degradation
Thermodynamics

ABSTRACT

Metallic coatings are widely employed to improve the oxidation resistance of superalloys. However, the interdiffusion between the metallic coatings and the superalloys leads to microstructural degradation in both. Some of the underlying degradation mechanisms are still elusive, e.g., the γ′ (Ni_3Al) phase depletion in superalloys, where a large amount of γ′ precipitates are dissolved in the γ matrix even though the incoming Al from coatings indeed increases the Al content. Here, we investigated the interdiffusion behavior between the Amdry365 coating and the IN792 superalloy at 1100 °C, using multiple microscopic techniques and thermodynamics calculations. Our results showed an excellent agreement between experiments and thermodynamics simulations, indicating the dominant role of Al on the initial diffusion-induced phase transitions. We proposed the Al-Cr interference effect to account for the pile-up behavior of Cr and the reduced Al content near the coating/superalloy interface. The local phase equilibrium calculations revealed that the γ′ depletion in the superalloy is primarily attributed to the loss of γ′-forming elements, such as Ta and Ti. Our findings opened up an avenue for studies on the superalloy/coating interdiffusion, contributing to reducing this damaging impact.

1. Introduction

Thermal barrier coatings (TBCs) significantly elevate the operating temperatures and enhance the oxidation resistance of superalloys, the state-of-the-art materials for high-pressure turbine blades in aircraft engines [1–4]. The functioning of TBCs is achieved through a ceramic top coating with low thermal conductivity, and a metallic bond coating to provide oxidation resistance [5–7]. MCrAlY coatings (M: Ni and/or Co) are widely employed as bond coatings due to their exceptional high-temperature oxidation resistance and cost-effectiveness [8–12]. In these systems, an approximate 50 vol% fraction of β-NiAl precipitates acts as Al reservoirs, enabling the formation of a dense Al_2O_3 layer as a barrier against oxygen penetration at elevated temperatures [13,14]. Additionally, a thermally grown Al_2O_3 layer on the bond coating mitigates the thermal expansion mismatch between the ceramic top coating and the substrate superalloy [15]. Unfortunately, interdiffusion often occurs between the bond coating and the superalloy at high temperatures, resulting in microstructural degradation of the superalloy [16–20]. Further, this effect compromises the high-temperature mechanical properties of the substrate superalloy. For example, coated superalloys, IN792, Superni C263 and K403, exhibit reduced creep or fatigue life compared to uncoated materials under identical testing conditions [21–24]. Hence, the advantage of bond coatings, i.e., enhanced oxidation resistance, comes at the expense of reduced mechanical properties.

The interdiffusion between the coating and the superalloy is driven by a chemical potential gradient. Driven by this, the elements of Al, Cr, Co migrate from the coating side to the superalloy side, while simultaneously the elements of Ta, W, Mo, Ti in the superalloy side diffuse to the coating side [25,26]. Notably, the elements of Al, Cr, Co exhibit higher diffusion rates compared to Ta, W, Mo, Ti in the nickel-based superalloy [27,28]. The discrepancy in elemental diffusion rates causes the formation of Kirkendall voids in the coating side, close to the coating/superalloy interface, thereby weakening the bonding between the coating and the superalloy [27,29]. Furthermore, the elemental diffusion disrupts the original phase equilibrium in both the superalloy and the coating. Consequently, it leads to the precipitation of topologically close

* Corresponding author.
E-mail address: ru.peng@liu.se (R.L. Peng).

https://doi.org/10.1016/j.matdes.2024.112937
Received 20 November 2023; Received in revised form 11 April 2024; Accepted 12 April 2024
Available online 12 April 2024

Table 1
Compositions of IN792 and Amdry365 (in wt.%).

	Al	Cr	Co	Y	Ta	W	Mo	Ti	C	Ni
IN792	3.4	12.5	9	–	4.2	4.2	1.9	4	0.08	Bal.
Amdry365	10.5	20.4	23.4	0.6	–	–	–	–	–	Bal.

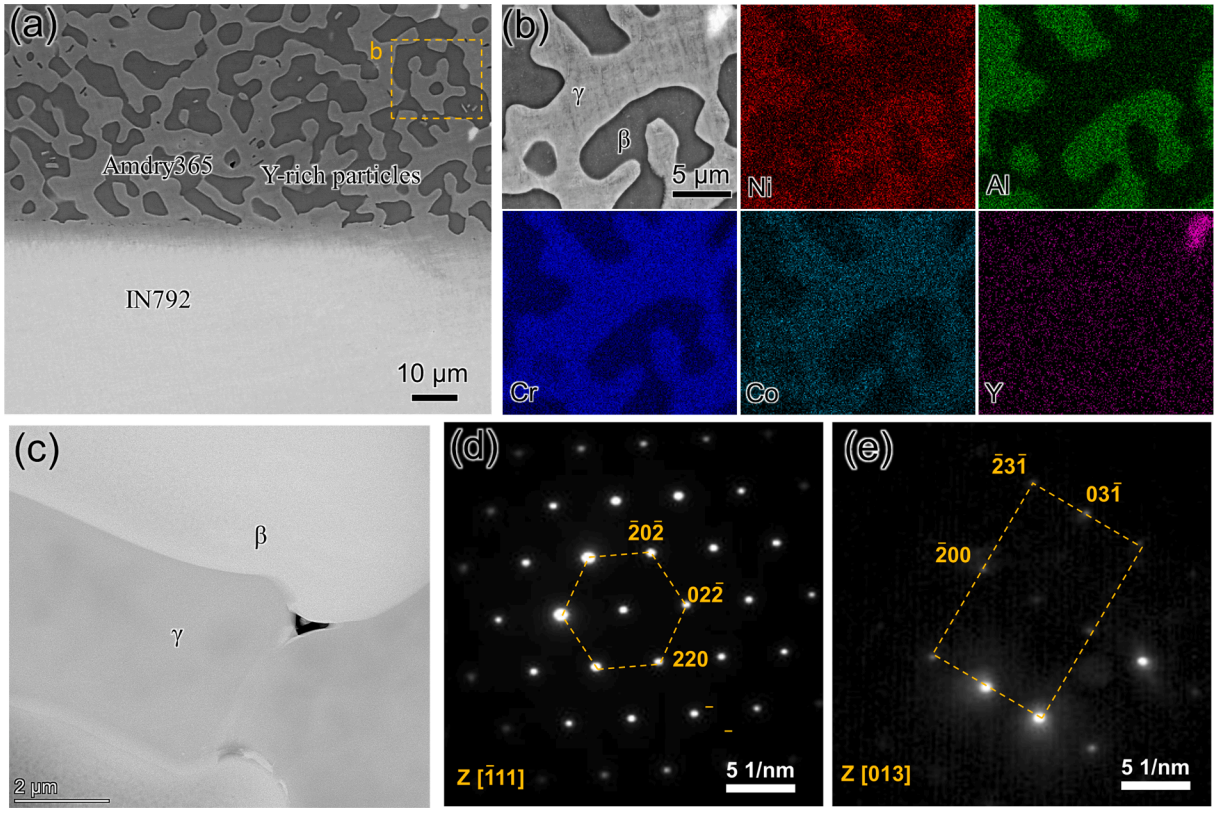

Fig. 1. The microstructure of Amdry365 after SPS. (a) SEM image; (c) the HAAD image; SADPs of (d) γ and (e) β phase.

packed (TCP) phases and the depletions of both β and γ′ phases [30–34]. Those brittle TCP phases, such as (Cr, Ta)-rich μ phase, (Al, W, Co)-rich P phase and (Cr, Co)-rich σ phase, could reduce the ductility of superalloys [35–37]. The β depletion (β → γ) can be attributed to the loss of Al, which is the primary component of both β (NiAl) and γ′ (Ni_3Al) [38]. However, the depletion of γ′ in superalloys is still elusive: while the incoming Al from the coating should in principle promote the precipitation of γ′ phase in the superalloy, numerous experimental observations confirm the formation of a γ′ depleted zone [16,31,39–41]. A comprehensive understanding of this phenomenon is crucial to reduce the adverse impact of bond coatings on superalloys.

In this research, we investigated the interdiffusion behavior between a classic MCrAlY coating Amdry365 and a nickel-based superalloy IN792, using an integrated approach combing microscopic techniques and thermodynamic calculations. IN792 is a typical high-Ti, Re-free superalloy, renowned for its exceptional high-temperature strength and cost-effectiveness [42]. Ti enhances the precipitation hardening effect [43,44], but diminishes the high-temperature oxidation resistance of superalloys [45,46]. Thus, a protective coating is necessary for this material. The oxidation test was carried out at 1100 °C for up to 2000 h in air. The microstructural evolution near the Amdry365/IN792 interface was examined by scanning electron microscopy (SEM) equipped with an energy dispersive spectroscopy (EDS), and the quantitative measurement of composition profiles was implemented using electron probe microanalysis (EPMA). The Thermo-Calc (TC) software was employed to simulate the interdiffusion process between Amdry365 and IN792.

2. Experiment and simulation

The chemical compositions of Amdry365 and substrate IN792 are provided in Table 1. The Amdry365 ingots with a size of 10 × 20 × 25 mm^3 were prepared using high purity (>99.9 %) pure metals by arc melting, in a water-cooled copper mold with an Ar protective atmosphere. The ingots were then sliced into thin sheets (0.5 × 20 × 25 mm^3), by the means of electrical discharge machining (EDM), and polished down to a thickness of 200 um finishing with #1200 SiC papers. IN792 substrates with a size of 5 × 20 × 25 mm^3 were sectioned from ingots via EDM and sequentially polished by #1200 SiC papers. Subsequently, Amdry365-IN792 couples were prepared using spark plasma sintering (SPS, SPS-825), under the compressive pressure of 30 MPa at 1000 °C for 20 min, in the evacuated chamber with a pressure of ~ 10^{-6} mbar. The couples were cut into six equal-sized pieces by EDM, as samples for the following oxidation tests. The oxidation tests were performed at 1100 °C in a muffle furnace for *t* h (*t* = 50, 200, 500, 900, 1400 and 2000). After cooling down to room temperature in ambient air, the oxidized specimens were embedded in conductive resins and polished, for microstructural observations.

The scanning electron microscope (SEM, Hitachi SU70 FEG) equipped with an energy dispersive X-ray spectrometer (EDS, Aztec Energy X-max 80) was employed to characterize the microstructure of initial Amdry365 ingots, resulting oxide layers and microstructural evolution

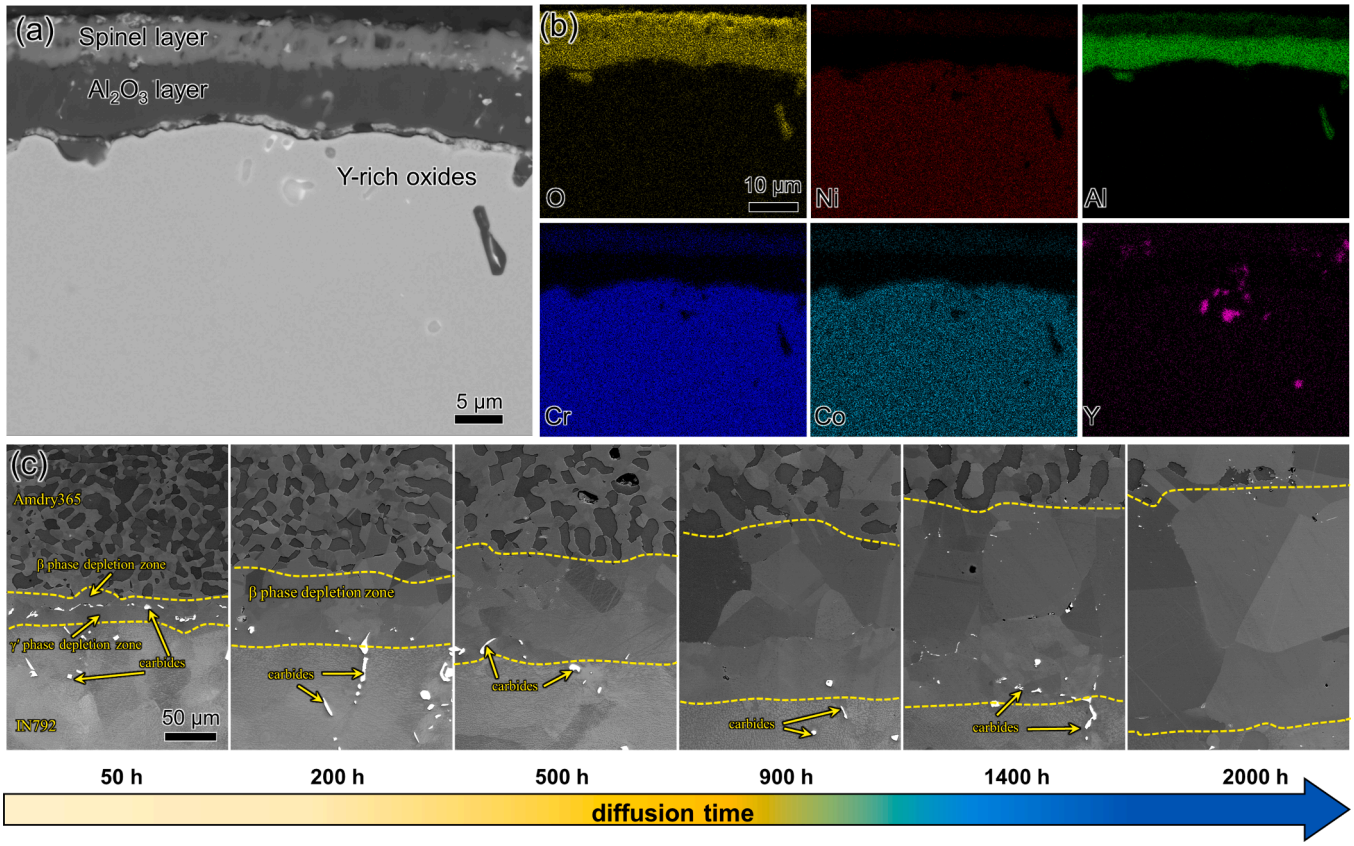

Fig. 2. (a) The cross-section microstructure and (b) the EDS elemental mapping of oxide layers on the surface of Amdry365 after 2000 h of oxidation at 1100 °C; (c) the microstructural evolution induced by interdiffusion between Amdry365 and IN792.

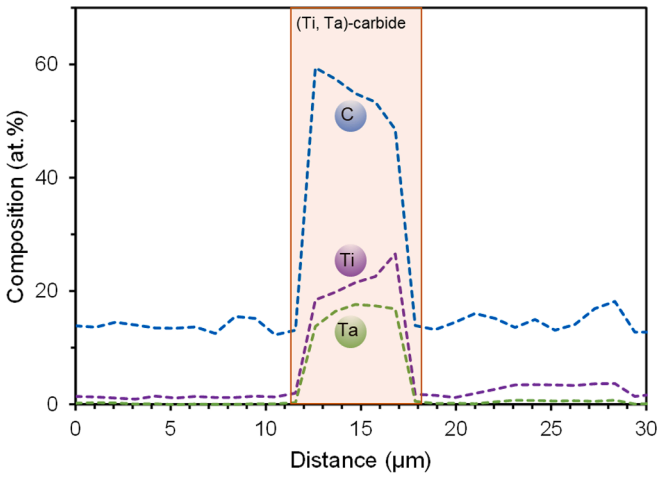

Fig. 3. The EDS line scan results on the formed carbides near the interface between Amdry365 and IN792.

due to interdiffusion between Amdry365 and IN792. The quantitative analysis of compositions was carried out by an electron probe micro-analyzer (EPMA, SHIMADZU1720H). The EPMA was operated at 15 keV and 10nA. EPMA, in contrast to EDS, distinguishes between elements based on the wavelengths of their characteristic x-ray emissions. This capability enables EPMA to discern contributions from elements that may 'overlap' when measured with EDS, thereby allowing for precise quantification of element concentrations, down to the ppm range [47]. The crystal structure of Amdry365 was identified by a transition electron microscope (TEM, Talos F200i). The TEM foils were prepared by twin-jet electropolishing in the electrolyte comprising 10 % perchloric acid and 90 % ethanol, at a temperature of −25 °C and a voltage of 20 V.

The thermodynamic calculations and diffusion simulations were performed using the Thermo-Calc software (TC, 2020b) with the TCNI10 and MOBNI5 database. The homogenization model #5 (upper Wiener bound) was applied to simulate the diffusion process using the diffusion-controlled transformation (DICTRA) module. System equilibrium was achieved by minimizing the total Gibbs free energy of the system, calculated by the property model3 (POLY3) module.

3. Results and discussions

3.1. Initial microstructure of Amdry365

The microstructure of Amdry365 after SPS was investigated by SEM, EDS and TEM (Fig. 1). Fig. 1a shows the microstructure of Amdry365, which is composed of ~ 49.5 vol% face-centered cubic phase (FCC, γ), ~50.5 vol% body-centered cubic phase (BCC, β), and a small amount of Y-rich particles. The phase fractions were measured by the image segmentation method based on the contrast of SEM images [48]. Fig. 1b illustrates the elemental distribution at the marked region of Fig. 1a, indicating the pile-up behavior of Ni and Al in the β phase, and of Co and Cr in γ, respectively. TEM analysis was applied to determine the crystal structure of Amdry365. A high-angle annular dark field (HAADF) TEM image is shown in Fig. 1c. Fig. 1d reveals the selected-area diffraction patterns (SADPs) with FCC diffraction spots along the [−1 1 1] zone axis, confirming that the dark phase in Fig. 1c is the γ phase. Fig. 1d shows the SADPs along the [0 1 3] zone axis, confirming that the bright phase has the BCC crystal constructure (β phase). It is noted that the contrast in the TEM image (Fig. 1c) is reversed to that in the SEM image (Fig. 1a).

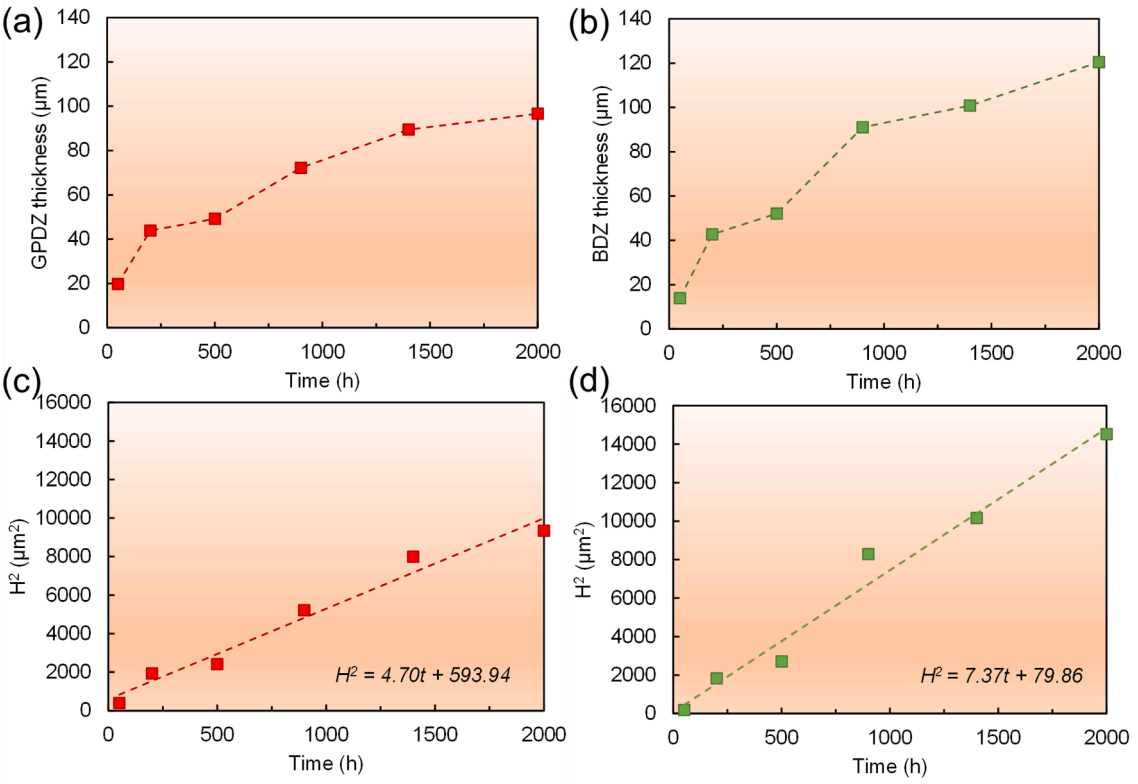

Fig. 4. The thickness changes of (a) GPDZ and (b) BDZ with increasing diffusion time. The square of thickness changes of (c) GPDZ and (d) BDZ as a function of diffusion time.

3.2. *The microstructural evolution induced by the coating/substrate interdiffusion*

Fig. 2a and 2b show the cross-sectional microstructure and the EDS elemental mapping of thermally grown oxides (TGOs) on the surface of Amdry365 after a 2000 h oxidation test at 1100 °C. Double oxide layers could be detected on the surface of oxidized Amdry365, including the outer $(Ni, Co, Cr, Al)_xO_y$ type spinel layer and the inner Al_2O_3 layer. The Al_2O_3 layer, as a dense barrier, has a crucial role in impeding the penetration of oxygen, due to its stable corundum structure, low Gibbs free energy of formation, low Pilling-Bedworth ratio (1.28) and non-volatility [49]. Furthermore, it is noteworthy that Y-rich oxides are scattered throughout these two oxide layers. Y, known as a reactive element, is reported to inhibit the cation diffusion along the oxide grain boundaries, thereby retarding the growth of oxide layers [50–52].

Fig. 2c shows the microstructural evolution induced by interdiffusion between Amdry365 and IN792 at 1100 °C. After 50 h, (Ta, Ti)-rich carbides could be detected at the interface between Amdry365 and IN792 (see Fig. 2c and Fig. 3). The diffusion of Al promotes the formation of carbides rich in Ta and Ti near the Amdry365/IN792 boundary, via improving the activities of Ta and Ti (see Fig. S1 in Supplementary materials). Subsequently, these carbides were dissolved in the matrix during the extended diffusion process. The depletion of β and γ′ is clearly shown, reflected by a β-depletion zone (BDZ) in the Amdry365 side and a γ′-depletion zone (GPDZ) in the IN792 side. The thickness changes (H) of GPDZ and BDZ are plotted as a function of diffusion time in Fig. 4a and Fig. 4b. The square of thickness changes (H^2) of both GPDZ and BDZ are proportional to the diffusion time (Fig. 4c and Fig. 4d). Thus, the growth of GPDZ and BDZ appears to follow the parabolic law. Both Amdry365 and IN792 are primarily composed with a two-phase system, namely, γ + β in Amdry365 and γ + γ′ in IN792. However, their interdiffusion could cause depletion of both γ′ and β. Our microstructural analysis indicates that their microstructural degradation initiates at the very early interdiffusion stage, and the prolonged microstructural evolution is a continuation of the initial phase transformation. Thus, modelling of interdiffusion during the early thermal exposure was performed using the DICTRA module of the Thermo-Calc software, to reveal the initial phase transformation mechanism induced by interdiffusion between Amdry365 and IN792.

3.3. *Interdiffusion simulation*

Fig. 5 shows the composition profiles (shown as open circles in red) measured by EPMA near the interface between Amdry365 and IN792 after 50 h. In both BDZ and GPDZ, the distribution of elements is continuous. However, in the two-phase regions of Amdry365 and IN792, the distribution of elements is discontinuous, which is attributed to the different composition of β, γ′ and γ phases. For example, Al is segregated in the β phase, and Cr and Co are segregated in the γ phase, as shown in the two-phase region of Amdry365 (Fig. 5a-5c). Moreover, the composition of each element in BDZ and GPDZ is close to that in the γ phase of the two-phase regions. where the concentration of Al is low.

The simulation results (represented by solid lines) compared with the EPMA results (shown as open circles in red) after 50 h are shown in Fig. 5. Notably, the simulation results show a noticeable pile-up behavior of Cr and Co and a low Al concentration in the BDZ and GPDZ regions, while these behaviors are not obvious in the measured results. This is due to the elemental segregated behavior, namely, Al is segregated in the β phase, Cr and Co are segregated in the γ phase, as shown in the two-phase region of Amdry365 (Fig. 5a-5c). The moving average method is employed to smooth the data as shown in supplementary material Fig. S2, indicating the agreed results with the simulation. And the pile-up behavior of Cr and Co can be verified in previous research [53,54].

A distinct kink is discernible at the interface between Amdry365 and IN792, which is ascribed to the lower diffusion rate of refractory metal

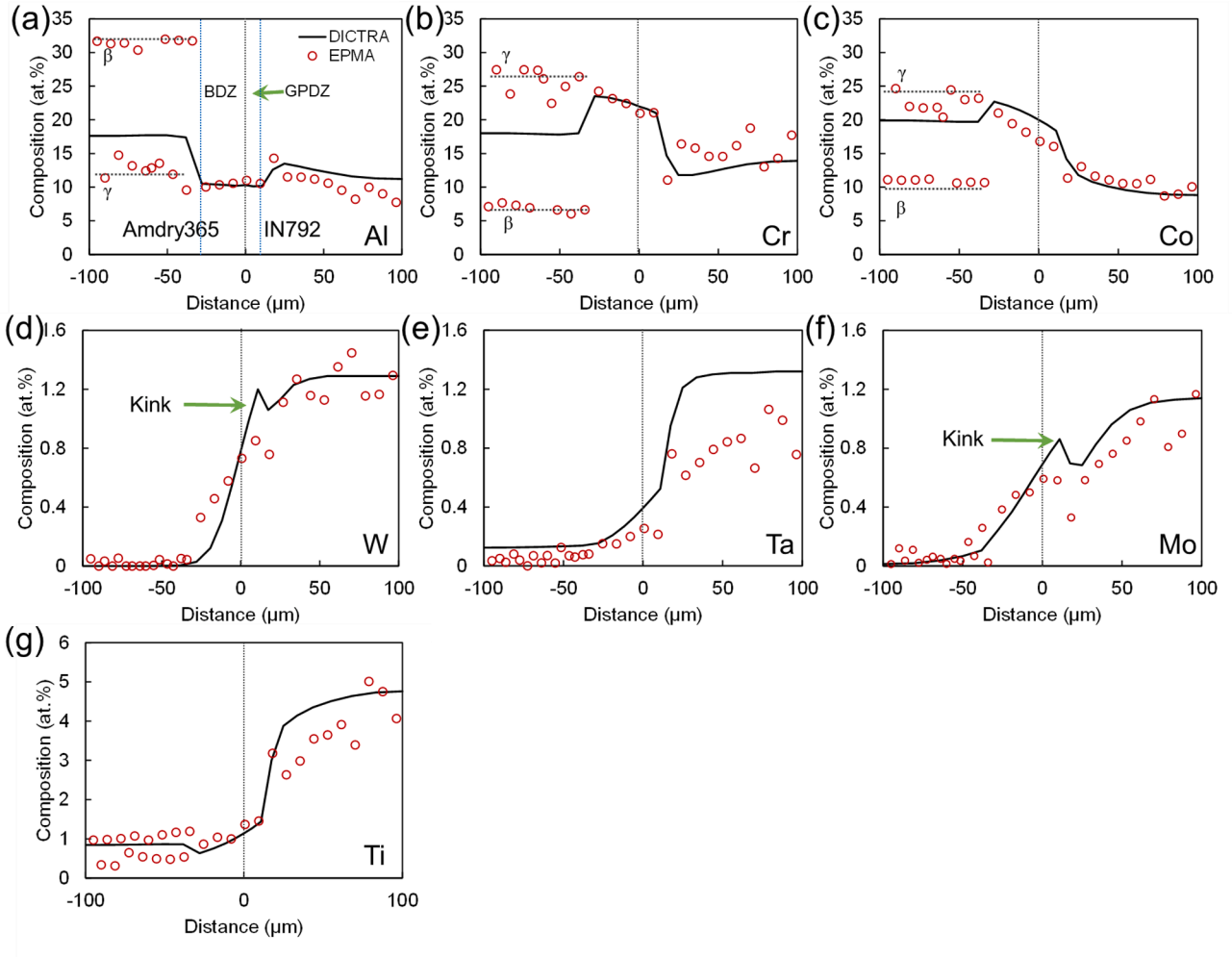

Fig. 5. The composition profiles of DICTRA simulation compared with the EPMA measured results, after the interdiffusion between Amdry365 and IN792 at 1100 °C for 50 h.

elements, specifically W and Mo, as also reported by Chyrkin et al. [29]. The measured concentrations of Ta and Ti are lower than the simulated results, since the formation of carbides consumes Ta and Ti elements.

Fig. 6 presents the diffusion simulation results of phase fraction, composition, and chemical potential of Cr at 1100 °C for the times of 2, 20 and 150 min, respectively, which correspond to three typical stages of different phase transformation processes. In the first stage, interdiffusion leads to the depletion of β precipitates in Amdry365, the formation of a ternary-phase region (β, γ′ and γ) near the Amdry365/IN792 interface, and the increment of the γ′ phase in IN792. These changes are primarily ascribed to the rapid migration of Al, with a high diffusion coefficient in the nickel-based matrix [28]. Although the detection of β phase isn't initially observed on the superalloy side since the coating/superalloy interdiffusion has occurred in the SPS process, it can be verified in the early interdiffusion process between Fe-containing coatings and IN792 (see supplementary material Fig. S3). The presence of Fe slows down the β depletion on the superalloy side [38]. The increment of γ′ phase fraction can be detected in supplementary material Fig. S4.

In the second stage, a significate pile-up of Cr can be detected in the ternary-phase region (see Fig. 6e). The Al and Cr contents are highly sensitive to each other's chemical potential (see Fig. 7a and 7b). Here, we refer such interdependence as the Al-Cr interference (ACI) effect. Due to this effect, the increasing Al content significantly elevates the Cr potential in the two-phase region (γ and γ′) of IN792 (see Fig. 6h). Driven by the chemical potential gradient, a great amount of Cr would diffuse to the ternary-phase region from both sides of the coating and the superalloy, resulting in the pile-up of Cr. Meanwhile, the increment of Cr elevates the chemical potential of Al in the ternary-phase region, which impedes the diffusion of Al from the coating side, while accelerating the inward diffusion of Al from this region to the inner region of IN792. Moreover, the ACI effect can be greatly influenced by the phase transition, such as the depletion of γ′, as shown in Fig. 7a, 7b, 7e and 7f.

In the third stage, the pile-up of Cr and Co, the decreasing content of Al, the loss of alloying elements Ta, Ti, Mo, W, and the formation of γ′ depletion zone, occur in the superalloy. While Co displays a pile-up behavior similar to Cr in the ternary-phase region (Fig. 6e and 6f), the mechanism behind it differs. As shown in Fig. 7b and 7d, the Co potential decreases with increasing Al content, which is different to the case of Cr. Therefore, the pile-up of Co cannot be explained by the blocking effect of Al. Instead, the effect of Cr is more sensitive to the chemical potential of Co. An increase in the Cr content reduces the potential of Co, promoting the diffusion of Co from the coating to the ternary-phase region, thereby resulting in the pile-up of Co [3]. The decreasing content of Al was ascribed to the pile-up of Cr, which further results in the depletion of β.

The γ′ depletion in the γ matrix could be caused by three potential origins: the decrease of Al, the loss of alloying elements of Ta, Ti, W, Mo, and the increment of Cr and Co. Firstly, the Al origin can be excluded, since the remained Al content near the Amdry365/IN792 interface is still higher compared with that in the inner region of IN792 (Fig. 5a and 6f). To reveal the effect of the other two origins on the phase transition, the local phase equilibrium at the interface of Amdry365/IN792 is

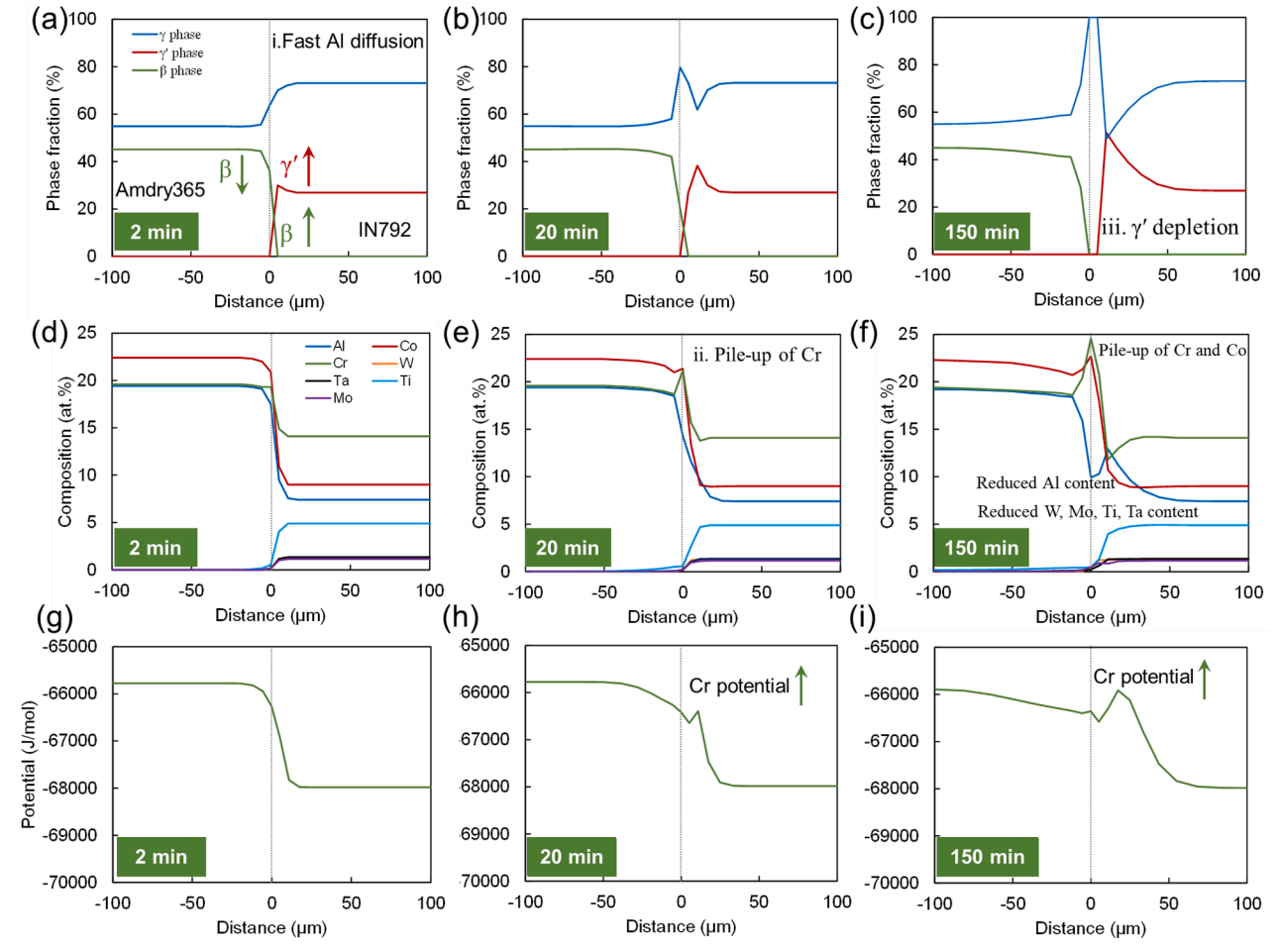

Fig. 6. The diffusion simulation results of (a-c) phase fraction, (d-f) composition and (g-i) chemical potential of Cr in the Amdry365/IN792 sample at 1100 °C, for the oxidation time of 2, 20 and 150 min, respectively.

calculated at 1100 °C with respect to composition variation in X (X = Co, Cr, Mo, W, Ta or Ti) and Al. As shown in Fig. 8a-8d, the $\gamma/(\gamma + \gamma')$ boundary is nearly parallel to the X axis, indicating that the phase transition from γ' to γ is almost independent of the Cr, Co, Mo and W contents. Thus, these elements have no contribution to the γ' dissolution. In comparison, the effects of Ta and Ti on the local phase equilibrium are significant (see Fig. 8e and 8f). For example, with the decrease of Ti from 4.9 to 0 at. %, the corresponding Al content at the $\gamma/(\gamma + \gamma')$ boundary is elevated from 4.74 to 12.69 at.%. This means that the loss of Ta and/or Ti will significantly decrease the stability of the γ' phase. In conclusion, the dissolution of γ' is primarily ascribed to the loss of Ti and Ta. Both elements stabilize γ' precipitates according to thermodynamics, thereby, their loss would promote the phase transition from γ' to γ. The consumption of Ti and Ta in the matrix of IN792 is caused by two ways, i.e., the formation of (Ti, Ta)-rich carbide and the diffusion of Ti and Ta from the superalloy side to the coating side. The formation of (Ti, Ta)-rich carbide cannot cause a wide range of γ' depletion, due to its small quantity (see Fig. 3c) and limited effect range (see supplementary materials Fig. S5). Moreover, the diffusion of Ti and Ta further leads to the dissolution of the carbide near the coating/superalloy boundary (see Fig. 3c). Hence, the effect of the resulting carbide is very limited to the formation of γ'-depletion zone, and the γ' depletion near Amdary365/IN792 interface is mainly attributed to the diffusion of Ta and Ti. This mechanism is quite different from those systems, such as β-NiAlPt/CMSX-4 [26] and β-Ni(CoPt)Al/Rene N5 [30], with excessive TCP or carbide particles formed. They break the original phase equilibrium of superalloys, causing the significant degradation of γ' precipitates.

The core findings in this research are summarized in Fig. 9 including: (i) the fast diffusion of Al leading to the β phase depletion of coatings and the formation of β, the γ' phase increment on the superalloy side; (ii) ACI effect, namely, the incoming Al improves the Cr potential, causing the diffusion of Cr from the inner of superalloys to the coating/superalloy interface, meanwhile the pile-up of Cr increases the Al potential, which accelerates the Al diffusion from this region into the inner of superalloys. (iii) γ' phase depletion in the substrate ascribed to the loss of γ' forming elements, Ti and Ta. This research clarifies a previous confusing point [31] that the reason for the γ' phase depletion is the increase of Cr, Co. These results answer a long-term-remained but critical question in the coating/superalloy interdiffusion research, i.e., why the γ' precipitates are dissolved in the γ matrix even though the incoming Al from coatings indeed increases the Al content. The γ' phase depletion is ascribed to loss of γ' forming elements, Ti and Ta, and the incoming Al cannot offset their effect. The simulation of diffusion used in this paper still requires a long calculation time, as a large number of elements were considered in the diffusion model. According to our findings, γ' depletion is mainly dependent on the loss of Ta, Ti. Hence, the simplified prediction model of γ' depletion for fast computation can be established by only considering the diffusion of Ta, Ti and Al.

4. Conclusions

In this work, we investigated the interdiffusion behavior between Amdry365 coating and IN792 superalloy at 1100 °C, using multiple microscopic techniques and thermodynamics calculations. The

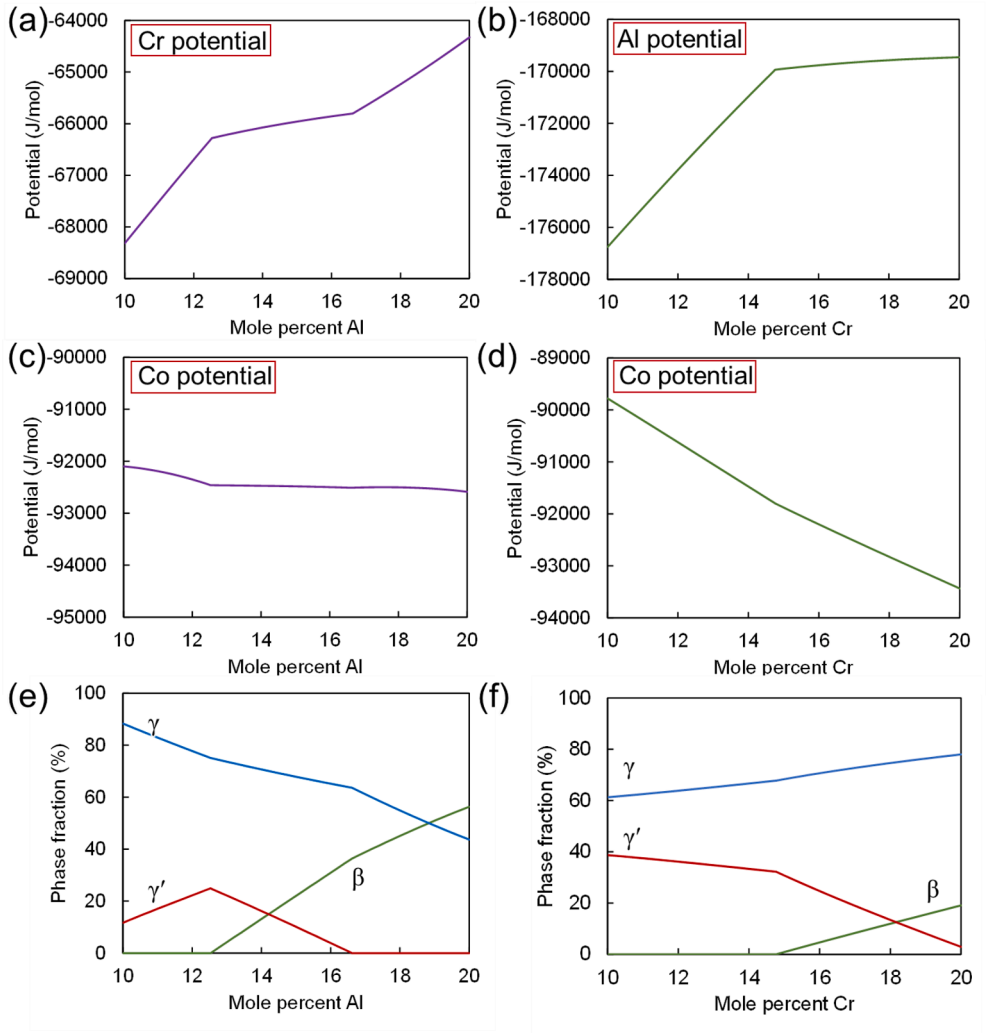

Fig. 7. The thermodynamics calculation results based on the compositions at the initial Amdry365/IN792 interface, showing (a-d) the chemical potential changes and (e-f) the phase transitions with the increasing content of Al or Cr.

following major conclusions can be reached.

(1) The depletions of β and γ′ were detected in Amdry365 and IN792, respectively, exhibiting a parabolic law with time. The thermodynamics simulations revealed the dominant effect of Al on the initial diffusion-induced phase transitions, causing the β depletion in Amdry365, and the formation of β and the increment of γ′ in IN792.
(2) Cr pile-up was observed near the Amdry365/IN792 interface, which was attributed to the increment of Al, which improved the chemical potential of Cr, and caused the diffusion of Cr from the inner region of IN792 to the Amdry365/IN792 interface. Also, the pile-up of Cr increased the chemical potential of Al, which accelerated the diffusion of Al from the ternary phase region to the inner region of IN792 and simultaneously retarded the incoming Al from the Amdry365 side. Moreover, the pile-up of Cr reduced the chemical potential of Co, resulting in the pile-up of Co.
(3) The local phase equilibrium calculations revealed that the γ′ depletion of superalloys is primarily attributed to the loss of γ′-forming elements, such as Ta and Ti. Our findings provided new insights for the interdiffusion between the superalloy and the coating, and on how to reduce the damage caused by it.

CRediT authorship contribution statement

Xiaoyu Sun: . **Xiaolong Li:** Writing – review & editing, Resources, Data curation. **Sheng Guo:** Writing – review & editing, Resources, Conceptualization. **Xin Yu:** Software, Resources, Data curation. **Lilong Zhu:** Resources, Data curation. **Jianwei Teng:** Resources, Data curation. **Liang Jiang:** Resources, Data curation. **Johan Moverare:** Supervision, Methodology. **Xin-Hai Li:** Supervision, Resources. **Ru Lin Peng:** Writing – review & editing, Software, Resources, Investigation, Funding acquisition, Conceptualization.

Declaration of competing interest

The authors declare that they have no known competing financial interests or personal relationships that could have appeared to influence the work reported in this paper.

Data availability

The authors do not have permission to share data. The raw/processed data required to reproduce these findings cannot be shared at this time as the data also forms part of an ongoing study.

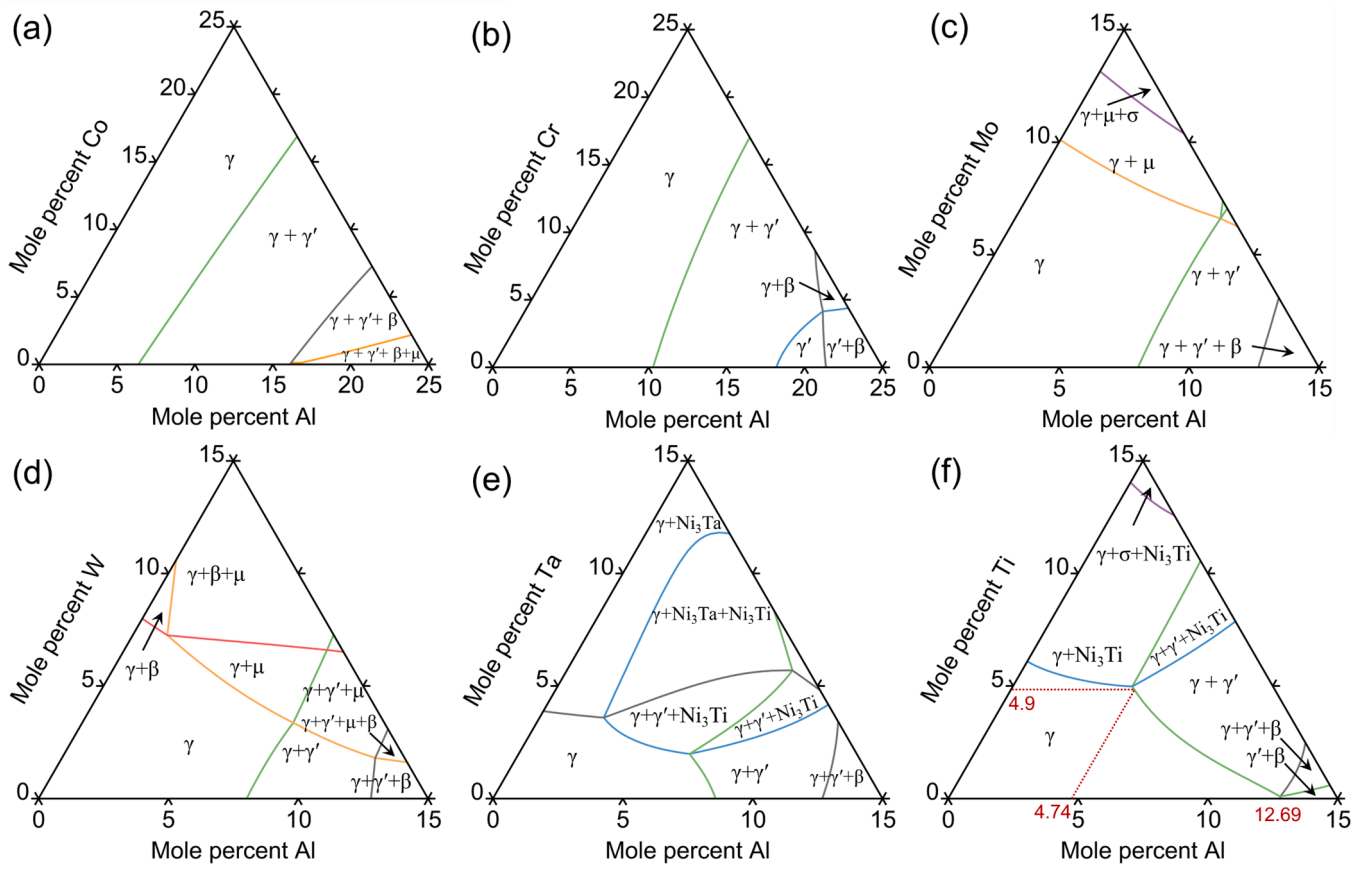

Fig. 8. The isothermal section calculated by the Thermo-Calc software at 1100 °C, showing the local phase equilibrium at the Amdry365/IN792 interface with respect to X (X = Co, Cr, Mo, W, Ta or Ti) and Al.

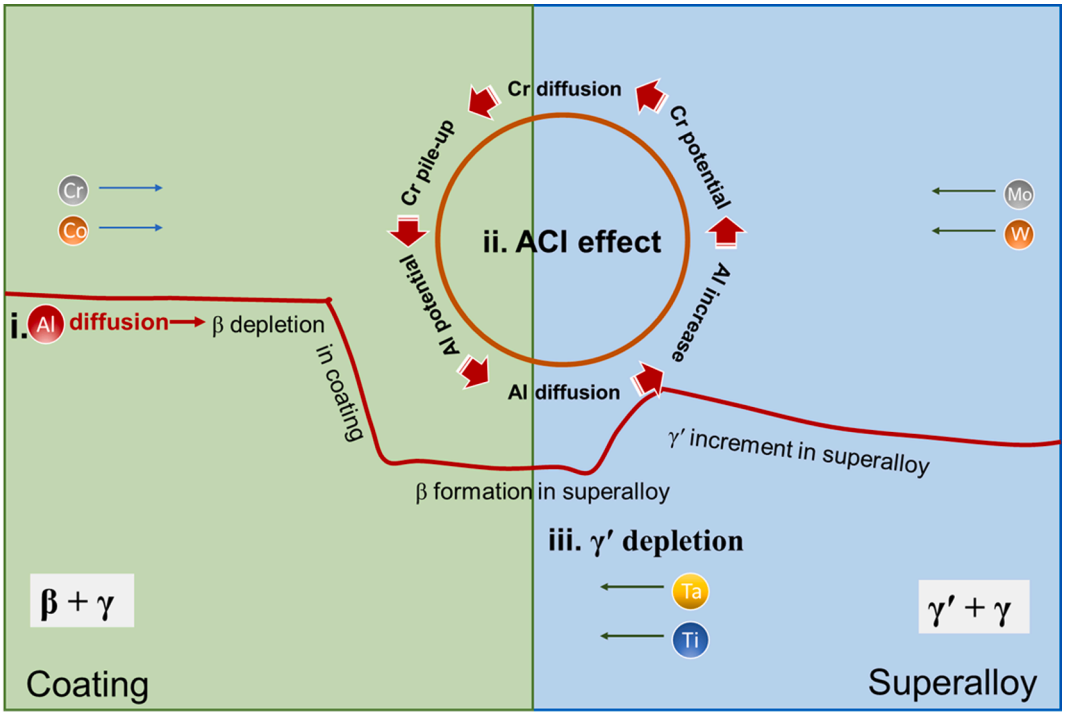

Fig. 9. The schematic diagram of Amdry365/IN792 interdiffusion mechanism indicating: (i) fast Al diffusion leading to the β depletion in the coating side and the β formation, the γ′ increment in the superalloy side; (ii) Al-Cr interference effect (ACI); (iii) γ′ depletion due to the loss of Ta and Ti.

Acknowledgements

The authors acknowledge the financial support from Siemens Industrial Turbomachinery AB (Finspång, Sweden) and Stiftelsen Axel Hultgrens Fond (Stockholm, Sweden). R. P. appreciates the Swedish Government Strategic Research Area in Materials Science on Functional Materials at Linköping University (Faculty Grant SFO-Mat-LiU 2009-00971) for financial support.

Appendix A. Supplementary data

Supplementary data to this article can be found online at https://doi.org/10.1016/j.matdes.2024.112937.

References

[1] G.W. Goward, Progress in coatings for gas turbine airfoils, Surf. Coat. Technol. 108–109 (1998) 73–79, https://doi.org/10.1016/S0257-8972(98)00667-7.
[2] N.P. Padture, M. Gell, E.H. Jordan, Thermal barrier coatings for gas-turbine engine applications, Science 296 (2002) 280–284, https://doi.org/10.1126/science.1068609.
[3] X. Sun, P. Zhang, J. Moverare, X. Li, L. Cui, R. Lin, Materials & Design Impeding the c 0 depletion during the interdiffusion between bond coatings and superalloys via introduction of tantalum in bond coatings, Mater. Des. 227 (2023) 111792, https://doi.org/10.1016/j.matdes.2023.111792.
[4] R.C. Reed, The Superalloys fundamentals and applications, Cambridge University Press, Cambridge, 2006. https://doi.org/10.1017/CBO9780511541285.
[5] A. Paksereshtt, F. Sharifianjazi, A. Esmaeilkhanian, L. Bazli, M. Reisi Nafchi, M. Bazli, K. Kirubaharan, Failure mechanisms and structure tailoring of YSZ and new candidates for thermal barrier coatings: A systematic review, Mater. Des. 222 (2022) 111044, https://doi.org/10.1016/j.matdes.2022.111044.
[6] G. Bolelli, M.G. Righi, M.Z. Mughal, R. Moscatelli, O. Ligabue, N. Antolotti, M. Sebastiani, L. Lusvarghi, E. Bemporad, Damage progression in thermal barrier coating systems during thermal cycling: A nano-mechanical assessment, Mater. Des. 166 (2019) 107615, https://doi.org/10.1016/j.matdes.2019.107615.
[7] L.Y. Lim, S.A. Meguid, Temperature dependent dynamic growth of thermally grown oxide in thermal barrier coatings, Mater. Des. 164 (2019) 107543, https://doi.org/10.1016/j.matdes.2018.107543.
[8] S.M. Li, L.B. Fu, W.L. Zhang, W. Li, J. Sun, T.G. Wang, S.M. Jiang, J. Gong, C. Sun, Formation process and oxidation behavior of MCrAlY + AlSiY composite coatings on a Ni-based superalloy, J. Mater. Sci. Technol. 120 (2022) 65–77, https://doi.org/10.1016/j.jmst.2021.10.055.
[9] Y. Chen, X. Zhao, P. Xiao, Effect of microstructure on early oxidation of MCrAlY coatings, Acta Mater. 159 (2018) 150–162, https://doi.org/10.1016/j.actamat.2018.08.018.
[10] A. Kalush, D. Texier, M. Ecochard, Q. Sirvin, K. Choquet, T. Gheno, N. Vanderesse, W. Jomaa, P. Bocher, Surface & Coatings Technology Size effects on high temperature oxidation of MCrAlY coatings processed via APS and HVOF depositions, Surf. Coat. Technol. 440 (2022) 128483, https://doi.org/10.1016/j.surfcoat.2022.128483.
[11] S. Xie, S. Lin, Q. Shi, W. Wang, C. Song, W. Xu, M. Dai, A study on the mechanical and thermal shock properties of MCrAlY coating prepared by arc ion plating, Surf. Coat. Technol. 413 (2021) 127092, https://doi.org/10.1016/j.surfcoat.2021.127092.
[12] D. Guo, Y. Wang, R. Fernandez, L. Zhao, B. Jodoin, Cold spray for production of in-situ nanocrystalline MCrAlY coatings – Part I: Process analysis and microstructure characterization, Surf. Coat. Technol. 409 (2021) 126854, https://doi.org/10.1016/j.surfcoat.2021.126854.
[13] P. Richer, M. Yandouzi, L. Beauvais, B. Jodoin, Oxidation behaviour of CoNiCrAlY bond coats produced by plasma, HVOF and cold gas dynamic spraying, Surf. Coat. Technol. 204 (2010) 3962–3974, https://doi.org/10.1016/j.surfcoat.2010.03.043.
[14] D. Toma, W. Brandl, U. Köster, Studies on the transient stage of oxidation of VPS and HVOF sprayed MCrAlY coatings, Surf. Coat. Technol. 120–121 (1999) 8–15, https://doi.org/10.1016/S0257-8972(99)00332-1.
[15] D. Texier, D. Monceau, Z. Hervier, E. Andrieu, Effect of interdiffusion on mechanical and thermal expansion properties at high temperature of a MCrAlY coated Ni-based superalloy, Surf. Coat. Technol. 307 (2016) 81–90, https://doi.org/10.1016/j.surfcoat.2016.08.059.
[16] M.C. Galetz, C. Oskay, S. Madloch, Microstructural degradation and interdiffusion behavior of NiAl and Ge-modified NiAl coatings deposited on Alloy 602 CA, Surf. Coat. Technol. 364 (2019) 211–217, https://doi.org/10.1016/j.surfcoat.2019.02.048.
[17] Y. Liu, M. Zou, H. Su, L. Geng, Y. Yu, W. Zheng, Y. Pei, S. Li, S. Gong, H. Zhang, Coating-associated microstructure evolution and elemental interdiffusion behavior at a Mo-rich nickel-based superalloy, Surf. Coat. Technol. 411 (2021), https://doi.org/10.1016/j.surfcoat.2021.127005.
[18] J.E. Morral, M.S. Thompson, Interdiffusion and coating design, Surf. Coat. Technol. 43 (44) (1990) 371–380, https://doi.org/10.1016/0257-8972(90)90089-U.
[19] D. Shi, J. Song, H. Qi, S. Li, X. Yang, Effect of interface diffusion on low-cycle fatigue behaviors of MCrAlY coated single crystal superalloys, Int. J. Fatigue 137 (2020) 105660, https://doi.org/10.1016/j.ijfatigue.2020.105660.
[20] O. Knotek, F. Loffler, W. Beele, Diffusion barrier design against rapid interdiffusion of MCrA1Y and Ni-base material, Surf. Coat. Technol. 61 (1993) 6–13, https://doi.org/10.1016/0257-8972(93)90194-S.
[21] Y. Liu, Y. Ru, H. Zhang, Y. Pei, S. Li, S. Gong, Coating-assisted deterioration mechanism of creep resistance at a nickel-based single-crystal superalloy, Surf. Coat. Technol. 406 (2021), https://doi.org/10.1016/j.surfcoat.2020.126668.
[22] A.K. Ray, E.S. Dwarakadasa, D.K. Das, V.R. Ranganath, B. Goswami, J.K. Sahu, J. D. Whittenberger, Fatigue behavior of a thermal barrier coated superalloy at 800 °C, Mater. Sci. Eng. A 448 (2007) 294–298, https://doi.org/10.1016/j.msea.2006.10.035.
[23] K. Yuan, R.L. Peng, X.H. Li, S. Johansson, Influence of precracked diffusion coating of Pt-modified aluminide on HCF fracture mechanism of IN792 nickel-based superalloy, Appl. Mech. Mater. 148–149 (2012) 24–29, https://doi.org/10.4028/www.scientific.net/AMM.148-149.24.
[24] L. Han, S. Zheng, M. Tao, C. Fei, Y. Hu, B. Huang, L. Yuan, Service damage mechanism and interface cracking behavior of Ni-based superalloy turbine blades with aluminized coating, Int. J. Fatigue 153 (2021) 106500, https://doi.org/10.1016/j.ijfatigue.2021.106500.
[25] Y. Zhang, J.P. Stacy, B.A. Pint, J.A. Haynes, B.T. Hazel, B.A. Nagaraj, Interdiffusion behavior of Pt-diffused $\gamma + \gamma'$ coatings on Ni-based superalloys, Surf. Coat. Technol. 203 (2008) 417–421, https://doi.org/10.1016/j.surfcoat.2008.08.053.
[26] P. Kiruthika, S.K. Makineni, C. Srivastava, K. Chattopadhyay, A. Paul, Growth mechanism of the interdiffusion zone between platinum modified bond coats and single crystal superalloys, Acta Mater. 105 (2016) 438–448, https://doi.org/10.1016/j.actamat.2015.12.014.
[27] C.E. Campbell, J.C. Zhao, M.F. Henry, Comparison of experimental and simulated multicomponent Ni-base superalloy diffusion couples, J. Phase Equilib. Diffus. 25 (2004) 6–15, https://doi.org/10.1361/10549710417966.
[28] C.E. Campbell, W.J. Boettinger, U.R. Kattner, Development of a diffusion mobility database for Ni-base superalloys, Acta Mater. 50 (2002) 775–792, https://doi.org/10.1016/S1359-6454(01)00383-4.
[29] A. Chyrkin, A. Epishin, R. Pillai, T. Link, G. Nolze, W.J. Quadakkers, Modeling interdiffusion processes in CMSX-10/Ni diffusion couple, J. Phase Equilib. Diffus. 37 (2016) 201–211, https://doi.org/10.1007/s11669-015-0444-9.
[30] N. Esakkiraja, A. Gupta, V. Jayaram, T. Hickel, S.V. Divinski, A. Paul, Diffusion, defects and understanding the growth of a multicomponent interdiffusion zone between Pt-modified B2 NiAl bond coat and single crystal superalloy, Acta Mater. 195 (2020) 35–49, https://doi.org/10.1016/j.actamat.2020.04.016.
[31] P. Zhang, X.H. Li, J. Moverare, R.L. Peng, The iron effect on oxidation and interdiffusion behaviour in MCrAlX coated Ni-base superalloys, Mater. Des. 166 (2019) 107599, https://doi.org/10.1016/j.matdes.2019.107599.
[32] P. Audigié, A. Rouaix-Vande Put, H. Murakami, D. Monceau, Chromium and iridium effects on the short-term interdiffusion behaviour between Pt rich γ-γ' bond-coatings and a Ni-Al-Cr alloy, Surf. Coat. Technol. 309 (2017) 258–265, https://doi.org/10.1016/j.surfcoat.2016.11.028.
[33] R.R. Adharapurapu, J. Zhu, V.S. Dheeradhada, D.M. Lipkin, T.M. Pollock, Effective Hf-Pd Co-doped β-NiAl(Cr) coatings for single-crystal superalloys, Acta Mater. 76 (2014) 449–462, https://doi.org/10.1016/j.actamat.2014.03.001.
[34] N. Czech, F. Schmitz, W. Stamm, Improvement of MCrAlY coatings by addition of rhenium, Surf. Coat. Technol. 68–69 (1994) 17–21, https://doi.org/10.1016/0257-8972(94)90131-7.
[35] R. Rettig, A. Heckl, R.F. Singer, Modeling of Precipitation Kinetics of TCP-Phases in Single Crystal Nickel-Base Superalloys, Adv. Mat. Res. 278 (2011) 180–185, https://doi.org/10.4028/www.scientific.net/AMR.278.180.
[36] Q. Li, S. Chen, Y. Zhang, C. Deng, L. Zhang, Stress-induced formation of μ-TCP phase during the early-stage interdiffusion process in the NiCrAlY/NiAlCoCrW model coating/superalloy system at ambient temperature, J. Alloy. Compd. 891 (2022) 161980, https://doi.org/10.1016/j.jallcom.2021.161980.
[37] C.A. Munson, G.M. Swain, Structure and chemical composition of different variants of a commercial trivalent chromium process (TCP) coating on aluminum alloy 7075–T6, Surf. Coat. Technol. 315 (2017) 150–162, https://doi.org/10.1016/j.surfcoat.2017.02.018.
[38] K. Ma, F. Tang, J.M. Schoenung, Investigation into the effects of Fe additions on the equilibrium phase compositions, phase fractions and phase stabilities in the Ni-Cr-Al system, Acta Mater. 58 (2010) 1518–1529, https://doi.org/10.1016/j.actamat.2009.10.059.
[39] M. Senge, J. Steger, A. Brückner-Foit, A. Rienäcker, Quantitative analysis of diffusion processes associated with γ'-depletion in Ni-base superalloys, Materialia 3 (2018) 41–49, https://doi.org/10.1016/j.mtla.2018.08.037.
[40] S. Salam, P.Y. Hou, Y.D. Zhang, H. Lan, H.F. Wang, C. Zhang, Z.G. Yang, Element accumulation beneath the scale/alloy interface of a CoNiCrAlReY alloy, Corros. Sci. 89 (2014) 318–325, https://doi.org/10.1016/j.corsci.2014.09.015.
[41] C.T. Liu, J. Ma, X.F. Sun, P.C. Zhao, Mechanism of the oxidation and degradation of the aluminide coating on the nickel-base single-crystal superalloy DD32M, Surf. Coat. Technol. 204 (2010) 3641–3646, https://doi.org/10.1016/j.surfcoat.2010.04.041.
[42] J. R. Davis, ASM specialty handbook: nickel, cobalt, and their alloys, ASM International, 2000. ISBN: 978-0-87170-685-0.
[43] J. Chen, J. Chen, Q. Wang, Y. Wu, Q. Li, C. Xiao, S. Li, Y. Wang, X. Hui, Enhanced creep resistance induced by minor Ti additions to a second generation nickel-based single crystal superalloy, Acta Mater. 232 (2022) 117938, https://doi.org/10.1016/j.actamat.2022.117938.
[44] S.I. Baik, S.Y. Wang, P.K. Liaw, D.C. Dunand, Increasing the creep resistance of Fe-Ni-Al-Cr superalloys via Ti additions by optimizing the B_2/L_{21} ratio in composite nano-precipitates, Acta Mater. 157 (2018) 142–154, https://doi.org/10.1016/j.actamat.2018.07.025.

[45] S.W. Yang, Effect of Ti and Ta on the oxidation of a complex superalloy, Oxid. Metal. 15 (1981) 375–397. https://link.springer.com/article/10.1007/BF0060353.
[46] J. Teng, X. Gong, B. Yang, S. Yu, J. Liu, Y. Li, Influence of Ti addition on oxidation behavior of Ni-Cr-W-based superalloys, Corros. Sci. 193 (2021) 109882, https://doi.org/10.1016/j.corsci.2021.109882.
[47] R. Rinaldi, X. Llovet, Electron Probe Microanalysis : A Review of the Past , Present , and Future Electron Probe Microanalysis : A Review of the Past , Present , and Future, (n.d.). https://doi.org/10.1017/S1431927615000409.
[48] X. Sun, L. Zhang, Y. Pan, X. Wang, Z. Huang, L. Jiang, Microstructural evolution during cyclic oxidation of a Ni-based singe crystal superalloy at 1100 °C, Corros. Sci. 162 (2019) 108216, https://doi.org/10.1016/j.corsci.2019.108216.
[49] N. Birks, G.H. Meier, F.S. Pettit, Introduction to the High Temperature Oxidation of Metals. Cambridge university Press, Cambridge, 2006. https://doi.org/10.2277/0521480426.
[50] B.A. Pint, Experimental observations in support of the dynamic-segregation theory to explain the reactive-element effect, 45 (1996) 1–37. https://link.springer.com/article/10.1007/BF01046818.
[51] R. Prescott, M.J. Graham, The formation of aluminum oxide scales on high-temperature alloys, Oxid. Met. 38 (1992) 233–254, https://doi.org/10.1007/BF00666913.
[52] T.J. Nijdam, W.G. Sloof, Effect of reactive element oxide inclusions on the growth kinetics of protective oxide scales, Acta Mater. 55 (2007) 5980–5987, https://doi.org/10.1016/j.actamat.2007.07.007.
[53] T. Galiullin, A. Chyrkin, R. Pillai, R. Vassen, W.J. Quadakkers, Effect of alloying elements in Ni-base substrate material on interdiffusion processes in MCrAlY-coated systems, Surf. Coat. Technol. 350 (2018) 359–368, https://doi.org/10.1016/j.surfcoat.2018.07.020.
[54] M. Elsaß, M. Frommherz, A. Scholz, M. Oechsner, Interdiffusion in MCrAlY coated nickel-base superalloys, Surf. Coat. Technol. 307 (2016) 565–573, https://doi.org/10.1016/j.surfcoat.2016.09.049.